hydrogen

MDPI

Article

Impact of Cathode Surface Area on Gas–Liquid Mass Transfer and Acetate Production Efficiency in H_2-Mediated Microbial Electrosynthesis from CO_2

Yuhan Guo [1], Menglong Zhao [1], Yan Yi [1], Jiahao Cao [1], Bingyan Wang [1], Hong Zhang [1], Wenfang Cai [1], Kai Cui [1,*], Sunil A. Patil [2] and Kun Guo [1,*]

[1] School of Chemical Engineering and Technology, Xi'an Jiaotong University, Xi'an 710049, China; gyh2001@stu.xjtu.edu.cn (Y.G.); a303870827@stu.xjtu.edu.cn (M.Z.); 3124116036@stu.xjtu.edu.cn (Y.Y.); cjhao@stu.xjtu.edu.cn (J.C.); wang_by@stu.xjtu.edu.cn (B.W.); zhang_hong@stu.xjtu.edu.cn (H.Z.); wenfang.cai@xjtu.edu.cn (W.C.)

[2] Department of ach Mohali (IISER Mohali), Sector 81, Knowledge City, SAS Nagar 140306, Punjab, India; sunil@iisermohali.ac.in

* Correspondence: cuikai212@xjtu.edu.cn (K.C.); kun.guo@xjtu.edu.cn (K.G.); Tel.: +86-029-8896-5843 (K.C. & K.G.)

Abstract

Hydrogen-mediated microbial electrosynthesis (MES) of chemicals from CO_2 relies on effective gas–liquid transfer at the cathode interface, yet the extent to which cathode surface area regulates acetate productivity remains insufficiently quantified. In this study, three identical MES reactors equipped with stainless-steel cathodes of different geometric areas (8×1, 8×4, and 8×16 cm^2) were operated at a constant electric current of 0.3 A. The largest cathode significantly accelerated hydrogen mass transfer (k_{La} = 0.592 h^{-1}), reaching dissolution equilibrium within 3 min, which was nearly twice as fast as the smallest electrode. Upon inoculation with enriched acetate-producing microbial consortia, the 8×16 $cm^2_{cathode}$ reactor fed with CO_2 achieved the highest steady-state acetate concentration of 32 $g \cdot L^{-1}$ produced at a rate of 2.12 $g \cdot L^{-1} \cdot d^{-1}$, with 94% hydrogen utilization, and 59% coulombic efficiency. In contrast, smaller electrodes exhibited rapid bubble detachment and reduced residence time, thereby limiting microbial gas uptake, and resulting in low acetate productivity. These findings demonstrate that cathode surface area is a key engineering lever controlling both hydrogen availability and electron recovery efficiency in H_2-driven MES. The results provide practical guidance for electrode design and scale-up of CO_2-to-acetate bioconversion via the MES process.

Keywords: microbial electrosynthesis; cathode surface area; gas–liquid mass transfer; hydrogen utilization; acetate production efficiency

Check for updates

Academic Editor: Rui C. Vilão

Received: 28 January 2026
Revised: 8 March 2026
Accepted: 19 March 2026
Published: 20 March 2026

Copyright: © 2026 by the authors. Licensee MDPI, Basel, Switzerland. This article is an open access article distributed under the terms and conditions of the Creative Commons Attribution (CC BY) license.

1. Introduction

The increasing urgency of carbon mitigation has driven extensive interest in sustainable carbon dioxide (CO_2) conversion technologies capable of transforming greenhouse gases into valuable chemicals while reducing atmospheric emissions [1,2]. Among these approaches, microbial electrosynthesis (MES) has emerged as a promising platform that couples renewable electricity with biological CO_2 fixation, enabling the conversion of CO_2 into multi-carbon compounds through microbial metabolism [3–6]. Unlike conventional electrochemical CO_2 reduction processes that rely on inorganic catalysts and often require high overpotentials or specific operating conditions [7–10], MES operates under

mild temperatures and pressures and primarily utilizes acetogenic microorganisms as biocatalysts [11–15]. These microorganisms employ the Wood–Ljungdahl pathway to convert CO_2 into acetate and other reduced products with high carbon selectivity [16]. In addition, microbial catalysts exhibit self-regeneration capability and relatively strong tolerance to impurities present in industrial gas streams, which can otherwise deactivate metal catalysts [17]. These advantages make MES particularly attractive for distributed carbon capture and utilization systems, especially when powered by renewable electricity sources such as solar or wind energy [18].

Within MES configurations, hydrogen-mediated systems have gained increasing attention due to their superior scalability compared to traditional biofilm-dependent systems based on direct electron transfer (DET) [19,20]. In DET systems, microorganisms must form and maintain active biofilms on the cathode surface in order to directly receive electrons, which often results in long start-up periods, limited biofilm thickness, and restricted electron transfer rates [21,22]. In contrast, hydrogen can serve as a soluble electron carrier, facilitating indirect electron transfer between the cathode and microbial cells. This mechanism effectively decouples microbial metabolism from attachment to the electrode surface, enabling more flexible reactor configurations [18]. This configuration allows uniform substrate distribution, simpler reactor design, and greater compatibility with external or in situ water electrolysis, making it more suitable for continuous and industrial operation [23].

Despite these advantages, the performance of hydrogen-mediated MES remains strongly constrained by gas–liquid mass transfer limitations [24]. Hydrogen formed at the cathode surface bio-electrochemically must dissolve efficiently before being utilized by microbes, yet rapid gas bubble detachment from the cathode and insufficient residence time in the bulk phase often leads to substrate loss and reduced productivity and coulombic efficiency. Previous studies have attempted to improve gas–liquid mass transfer in MES systems through various strategies, such as adding gas vectors to enhance hydrogen solubility [25], modifying electrode surfaces to reduce bubble diameter [26], and extending gas retention time using bubble column reactors [18]. However, one critical engineering parameter—cathode geometric surface area—has not been systematically examined. Since cathode size directly affects bubble nucleation density, detachment dynamics, and interfacial contact, its influence on hydrogen availability and acetate productivity remains poorly quantified.

To this end, we constructed three identical MES reactors equipped with stainless-steel cathodes of different surface areas and evaluated their performance under identical operating conditions. By analyzing gas bubble behavior, hydrogen dissolution kinetics, acetate production, and coulombic efficiency, this study elucidates how cathode area governs gas–liquid transfer and hydrogen-mediated CO_2 bioconversion performance. The results demonstrate that cathode surface area is not merely a structural component but a key tunable parameter for optimizing hydrogen-mediated MES. These findings offer practical guidance for the design and scale-up of CO_2-to-acetate MES reactors.

2. Materials and Methods

2.1. MES Reactor Construction

A 1.0 L sleeve-type continuous stirred-tank reactor (CSTR) was constructed, consisting of a double-jacketed glass cathode chamber (inner diameter 10.7 cm, height 14.5 cm) and a centrally positioned tubular anode compartment (Figure 1). The jacket was connected to a circulating water bath for temperature control. A magnetic stirrer placed at the bottom ensured homogeneous mixing of the liquid. The anode compartment was vertically mounted at the center of the reactor lid and comprised a cylindrical cation exchange membrane (CEM, 3.5 cm diameter, 12.5 cm height, CMI-7000, Membranes International Inc.,

Ringwood, NJ, USA) that enclosed an IrO_2-coated titanium mesh anode (3.2 × 8 cm^2, Baoji Zhiming Special Metal Co., Ltd., Baoji, China). Electrical terminals and replenishment ports were sealed with a gas-tight nylon cable gland to prevent leakage and oxygen intrusion.

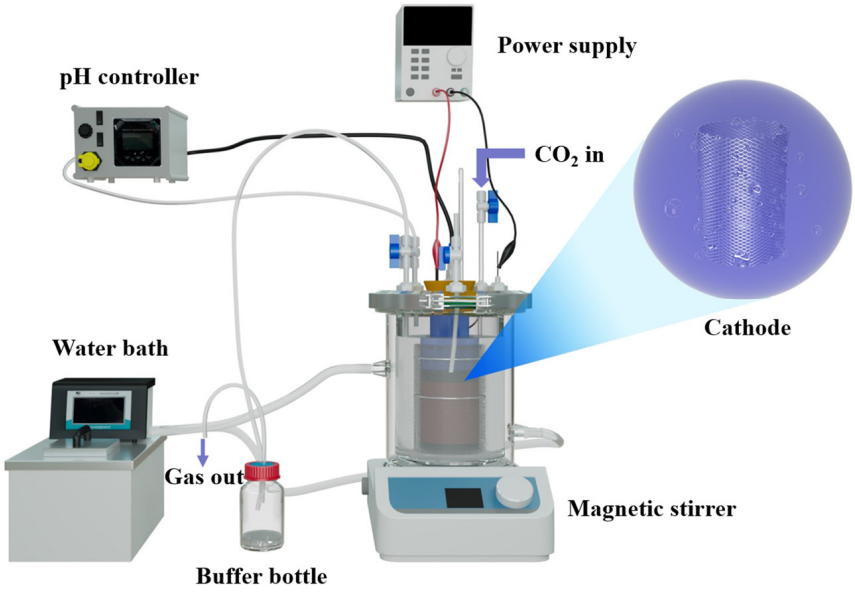


Figure 1. Schematic of the CSTR-configuration MES system along with accessories.

Stainless-steel mesh plates (Anguo Chengli Metal Co., Ltd., Baoding, China) with identical heights of 8 cm but different widths (1, 4, and 16 cm) were employed as cathodes, corresponding to projected surface areas of 8 cm^2, 32 cm^2, and 128 cm^2, respectively. The use of electrodes with identical heights but varying widths allowed systematic variation in the cathode surface area while minimizing differences in electrode geometry and hydrodynamic conditions. All cathodes were vertically installed in the reactor and positioned at the same distance from the anode to ensure consistent electrode spacing and comparable mass-transfer environments across the three reactors. The electrodes were connected to a regulated DC power supply, with the anode connected to the positive terminal and the cathode connected to the negative terminal to drive the electrochemical reactions. Each reactor lid was equipped with six functional ports that facilitated the introduction and monitoring of operational components, including a CO_2 inlet tube, an alkali dosing tube for pH regulation, a pH probe port for continuous monitoring, a sampling port for liquid analysis, an effluent outlet, and an electrode connection port.

To ensure strict anaerobic conditions during reactor operation, all ports and connections were tightly sealed using O-rings and stainless-steel clamps. This sealing configuration effectively prevented gas leakage and external oxygen intrusion, thereby maintaining a stable anaerobic environment suitable for microbial electrosynthesis.

2.2. Operating Conditions for the MES Reactor

2.2.1. Compositions of the Anolyte and Catholyte

The working volume of the reactor anolyte was 100 mL and consisted of a phosphate-buffered solution containing 3 $g \cdot L^{-1}$ KH_2PO_4 and 6 $g \cdot L^{-1}$ Na_2HPO_4. This buffer system was used to maintain a stable pH and provide sufficient ionic conductivity for anodic electrochemical reactions. The catholyte had a working volume of 600 mL and was prepared using a modified M9 medium designed to support the growth and metabolic activity of acetogenic microorganisms. The medium contained 3 $g \cdot L^{-1}$ KH_2PO_4, 6 $g \cdot L^{-1}$ Na_2HPO_4, 0.5 $g \cdot L^{-1}$ NH_4Cl as the nitrogen source, 0.1 $g \cdot L^{-1}$ $MgSO_4 \cdot 7H_2O$, 0.5 $g \cdot L^{-1}$ NaCl, and 14.6 $mg \cdot L^{-1}$ $CaCl_2$. In addition, 1 $mL \cdot L^{-1}$ vitamin solution and 1 $mL \cdot L^{-1}$ trace element

solution were added to supply essential micronutrients required for microbial growth and enzymatic activity.

To selectively promote acetogenic metabolism and suppress competing methanogenic archaea, sodium 2-bromoethanesulfonate was added to the catholyte at 2 mol·L^{-1}. The detailed compositions of the trace element and vitamin solutions are shown in Table S1 (Supplementary Material). All chemicals mentioned above are sourced from Sinopharm Group, Shanghai, China. Prior to reactor operation, the initial pH of both the anolyte and catholyte was adjusted to 7.0 to provide suitable conditions for microbial activity and electrochemical reactions.

2.2.2. Reactor Operating Parameters

Three MES reactors, each equipped with cathodes of different surface areas, were operated simultaneously. The temperature was maintained at approximately 35 °C using a circulating water bath, while the pH in the cathode chamber was controlled at 7 via a pH controller. The magnetic stirrer speed was set to 900 rpm. The reactors were operated in a constant-current mode at 0.3 A. Simultaneously, CO_2 was fed to the reactors at a rate of 1.2 mL·min^{-1}, maintaining a molar ratio of H_2:CO_2 at 2:1. Initially, all three reactors were operated under abiotic conditions for 12 h to thoroughly remove dissolved oxygen from the cathode solution. Subsequently, a mixed microbial consortium dominated by *Acetobacterium* species [25] for acetate production from CO_2 was inoculated into the catholyte of each reactor. The inoculum source and inoculation volume were identical across all three reactors to ensure no variables other than cathode area were present.

During reactor operation, 2 mL of liquid was sampled from the cathode chamber every 24 h to measure volatile fatty acid content and bacterial concentration, while replenishing the catholyte with an equal volume of fresh medium. The reactor gas outlet was connected to a water displacement column (containing 1 mmol·L^{-1} HCl solution) to collect reactor off-gases. This study employed a batch operation method for two cycles. Once the acetate concentration stabilized, 90% of the cathode solution was replaced with fresh medium to initiate a new batch cycle.

2.3. Analyses and Calculations

2.3.1. Gas Sample Analysis

A gas chromatograph (GC 7890B) equipped with both a thermal conductivity detector (TCD) and a flame conductivity detector (FCD) was employed to analyze the composition and concentrations of unreacted gases in the reactor. High-purity helium served as the carrier gas at a flow rate of 69 mL·min^{-1}. The inlet, column, and detector temperatures were maintained at 90 °C, 250 °C, and 250 °C, respectively.

2.3.2. Liquid Sample Analysis

After centrifugation, the supernatant of the liquid sample was collected and acidified with formic acid. Acetate concentration was determined using a gas chromatograph (GC 8860) equipped with a flame ionization detector (FID) and a capillary column. High-purity nitrogen served as the carrier gas at a constant flow rate of 25 mL·min^{-1}. The injector and detector temperatures were maintained at 250 °C. The column temperature program was as follows: (1) initial temperature 40 °C; (2) ramp to 170 °C at 15 °C·min^{-1}; (3) ramp to 240 °C at 20 °C·min^{-1}.

2.3.3. Determination of H_2 Mass Transfer Coefficient

The volumetric mass transfer coefficient (k_{La}) for H_2 was determined using the dynamic gassing method [27]. The cathode chamber of the reactor contained no fresh culture medium, and both temperature and pH were maintained at 35 °C and 7, respectively. A

dissolved hydrogen probe was placed in the cathode solution to monitor H_2 concentration. Prior to measurement, nitrogen gas was introduced to remove residual dissolved H_2. Experiments were conducted at a constant current of 0.3 A, and dissolved hydrogen readings were recorded every 10 s.

2.3.4. Imaging of H_2 Bubbles on the Cathode Surface

The reactor was filled with fresh bacteria-free culture medium, and electrolysis was conducted at a constant current of 0.3 A, identical to the operating conditions used in the biotic MES experiments. A high-speed camera (FASTCAM Mini UX100, equipped with a Nikon AF Micro-Nikkor 105 mm f/2.8G IF-ED lens) was employed to capture hydrogen bubble formation and detachment on the cathode surface in situ during electrolysis. The image acquisition duration was 2 s. To ensure the reliability and representativeness of the data, approximately 4000 images were captured for each cathode area, from which frames with consistent electrolysis time, clear bubble contours, and no overlapping interference were selected for analysis.

2.3.5. Calculations

The acetate production rate was calculated using Equation (1):

$$P_{HAc,t} = \frac{C_{HAc,t_{n+1}} - C_{HAc,t_n}}{t_{n+1} - t_n} \quad (1)$$

where $C_{HAc,tn+1}$ ($g \cdot L^{-1}$) is the acetate concentration at time tn+1, $C_{HAc,tn}$ ($g \cdot L^{-1}$) is the acetate concentration at time t_n, and tn+1−tn denotes the time interval (days).

The volumetric mass transfer coefficient (k_{La}) for H_2 was determined by data fitting according to the adsorption model (Equation (2)) [28]:

$$\frac{dC}{dt} = k_{La}(C^* - C) \quad (2)$$

where C* ($mg \cdot H_2 \cdot L^{-1}$) is the saturated concentration of dissolved hydrogen, t (h) is time, k_{La} ($cm \cdot h^{-1}$) is the volumetric mass transfer coefficient, and a ($cm^2 \cdot cm^{-3}$) is the ratio of gas–liquid interfacial area to liquid volume.

The coulombic efficiency (CE), which reflects electron recovery in the target product (i.e., acetate), was calculated using the following equation (Equation (3)):

$$CE = \frac{\Delta C_{HAc} \times V_{solution} \times 8 \times F}{Q_{total}} \times 100\% \quad (3)$$

where ΔC_{HAc} ($mol \cdot L^{-1}$) represents the change in acetate concentration during the experiment, $V_{solution}$ (L) is the cathode chamber solution volume, Q_{total} (C) is the total charge transferred through the cathode, and F is the Faraday constant.

3. Results and Discussion

3.1. Impact of Cathode Surface Area on Hydrogen Mass Transfer

The hydrogen mass transfer performance of reactors with different cathode areas is presented in Figure 2. At a current of 0.3 A, the reactor with the largest cathode area ($8 \times 16\ cm^2$) exhibited the fastest approach to dissolution equilibrium, reaching a maximum dissolved hydrogen concentration of 1.27 $mg \cdot L^{-1}$ within approximately 3 min. In comparison, the medium cathode area reactor ($8 \times 4\ cm^2$) reached a maximum concentration of 1.26 $mg \cdot L^{-1}$ after 4 min, while the smallest cathode area reactor ($8 \times 1\ cm^2$) reached 1.25 $mg \cdot L^{-1}$ after more than 6 min.

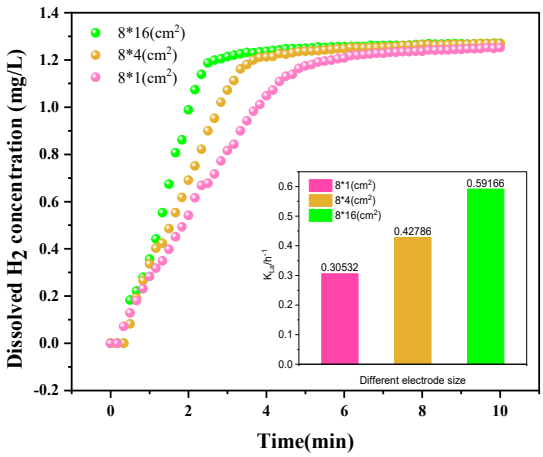


Figure 2. Dissolved H_2 concentration and k_{La} (inset) for reactors with different cathode areas: 8 × 1 cm^2, 8 × 4 cm^2, and 8 × 16 cm^2. (* in figure indicates a multiple sign).

Figure 2 also shows the calculated volumetric mass transfer coefficient (k_{La}). The reactor with the largest cathode area achieved a k_{La} value of 0.592 h^{-1}, nearly double that of the smallest cathode reactor, with k_{La} values increasing progressively with cathode area. This enhancement can be attributed to prolonged bubble residence times and more uniform bubble distribution in larger cathode systems. These findings clearly demonstrate that expanding the cathode area significantly improves hydrogen mass transfer performance, which is desired in MES reactors.

3.2. Impact of Cathode Surface Area on Hydrogen Bubble Formation

Figure 3 illustrates the distinct bubble behaviors observed in reactors with different cathode areas under identical electric current conditions. In the reactor with the smallest cathode area (Figure 3a), bubbles detached rapidly from the cathode surface immediately after the onset of electrolysis. Although the bubbles were relatively small in size, they had short residence times and ascended quickly through the liquid phase. In contrast, the reactor with the largest cathode area (Figure 3c) generated larger bubbles with prolonged detachment times, allowing them to remain attached to the electrode surface for an extended duration. The reactor with the medium cathode area (Figure 3b) displayed intermediate behavior, characterized by rapid bubble detachment at the electrode edges and a non-uniform distribution of bubble size across the surface.

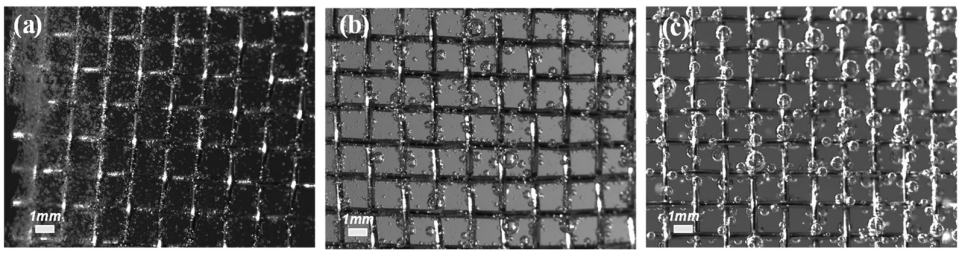


Figure 3. Representative images displaying bubble behavior on cathode surfaces with different cathode areas: 8 × 1 cm^2 (**a**), 8 × 4 cm^2 (**b**), and 8 × 16 cm^2 (**c**).

In the present study, reactors with smaller cathode areas produced numerous small bubbles that detached rapidly from the electrode surface. Although smaller bubbles generally provide larger specific interfacial areas, their short residence time limits effective hydrogen dissolution. In contrast, reactors with larger cathode areas generated bubbles that remained attached for longer times, thereby increasing bubble retention time and improving hydrogen availability for microbial utilization. In addition, larger cathode

surface areas promoted a more uniform distribution of hydrogen bubbles within the reactor. The extended bubble residence time and improved spatial distribution of desorbed bubbles significantly enhanced the hydrogen mass transfer coefficient [29]. These results suggest that smaller bubbles do not necessarily lead to higher gas–liquid mass transfer efficiency. Instead, an optimal combination of bubble size, residence time, and spatial distribution is required to achieve efficient hydrogen utilization in H_2-mediated MES systems.

3.3. Impact of Cathode Surface Area on Acetate Production in MES Reactors

Under identical inoculum sources and operating conditions, three reactors with different cathode areas were operated simultaneously for approximately 14 days over two successive batch cycles. The time-dependent variation in acetate concentration is shown in Figure 4a. In Batch 1, following inoculation with the acetate-producing microbial culture, all reactors exhibited a slow increase in acetate concentration during the first two days, remaining below 2 $g{\cdot}L^{-1}$ in the start-up phase. A marked increase occurred on day 3, indicating successful initiation of microbial activity. From this point onward, the reactor with the largest cathode area (8 × 16 cm^2) showed the fastest acetate accumulation, reaching 24 $g{\cdot}L^{-1}$ by day 12 and stabilizing thereafter. The reactor with a medium cathode area (8 × 4 cm^2) gradually stabilized at 18 $g{\cdot}L^{-1}$ on day 13, while the smallest cathode reactor (8 × 1 cm^2) stabilized at 16 $g{\cdot}L^{-1}$. The second batch displayed similar concentration profiles but with a shorter start-up period, likely due to the acclimatization and enhanced activity of the acetate-producing culture after repeated fermentation cycles. Consequently, notable differences among the three reactors only became evident from day 8 onward. Ultimately, the reactor with the largest cathode area (8 × 16 cm^2) achieved the highest steady-state acetate concentration of 32 $g{\cdot}L^{-1}$.

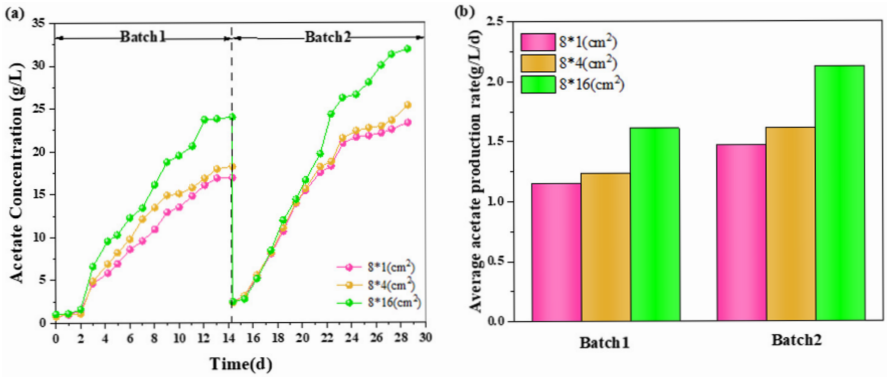


Figure 4. Acetate concentration trends over two batch cycles (**a**) and average acetate production rates (**b**) of MES reactors with cathodes with different surface areas: 8 × 1 cm^2, 8 × 4 cm^2, and 8 × 16 cm^2 (* in figures indicates a multiple sign).

Figure 4b presents the average acetate production rates across the three reactors. A clear positive correlation was observed between cathode area and production rate. In Batch 1, the reactor with an 8 × 16 cm^2 cathode area achieved an average rate of 2.12 $g{\cdot}L^{-1}{\cdot}d^{-1}$, while the 8 × 4 cm^2 and 8 × 1 cm^2 reactors reached 1.77 $g{\cdot}L^{-1}{\cdot}d^{-1}$ and 1.57 $g{\cdot}L^{-1}{\cdot}d^{-1}$, respectively. Although microbial activity was higher in Batch 2, leading to improved overall productivity, the relative acetate production trend remained consistent among all reactors.

It is noteworthy that the final acetate yields of the reactors with 8 × 1 cm^2 and 8 × 4 cm^2 cathodes differed only marginally. This outcome can be attributed to the hydrogen bubble release and utilization mechanism described in Section 3.2, where the combined effect of bubble size, residence time, and microbial capture efficiency governs hydrogen availability for acetogenesis. Furthermore, increasing the area of the cathode may lead

to an increase in device size and an increase in manufacturing costs, thereby limiting the large-scale application of this process. However, from the perspective of process efficiency, moderately expanding the area of the cathode can significantly improve the space–time yield of the reactor, and enhance the energy consumption level per unit capacity and the overall economic performance.

3.4. Impact of Cathode Surface Area on Gas Uptake Efficiency by Microbes

Figure 5a presents the time-dependent changes in H_2 utilization rates across the three MES reactors. In Batch 1, utilization increased sharply during the first three days, after which distinct differences emerged among reactors. The largest cathode area reactor (8×16 cm^2) achieved a peak utilization rate of 94%, stabilizing before gradually declining after day 12. This decrease can be attributed to product inhibition, where excessive acetate accumulation suppresses microbial activity, thereby reducing hydrogen consumption efficiency [30]. The reactors with 8×4 cm^2 and 8×1 cm^2 cathodes displayed similar utilization profiles, but with lower peak values of 84% and 83%, respectively, confirming that reduced cathode area limits effective H_2 utilization. In Batch 2, the reactor with the largest cathode area again maintained the highest gas utilization throughout operation. Interestingly, in the later stages, the smallest cathode area reactor exhibited slightly higher utilization than the intermediate cathode reactor, a trend consistent with the acetate concentration patterns. Nonetheless, the overall relationship remained unchanged: H_2 utilization decreased progressively as the cathode area decreased.

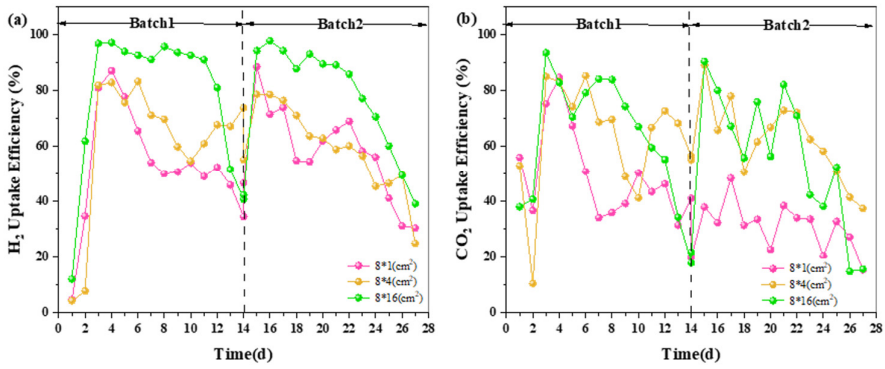


Figure 5. H_2 uptake efficiency (**a**) and CO_2 uptake efficiency (**b**) during MES reactor operation over two batch cycles with different cathode areas: 8×1 cm^2, 8×4 cm^2, and 8×16 cm^2 (* in figures indicates a multiple sign).

Figure 5b shows CO_2 utilization rates during reactor operation. In Batch 1, CO_2 utilization was low during the initial two days as the reactors were in the startup phase. Utilization rates for all three reactors increased rapidly on the third day, confirming successful startup. The reactor with a cathode area of 8×16 cm^2 achieved the highest CO_2 utilization rate of up to 93%, subsequently stabilizing around 85% before gradually declining after Day 8. The reactors with cathode areas of 8×4 cm^2 and 8×1 cm^2 achieved maximum CO_2 utilization rates of 85% and 84%, respectively. These results indicate that the reactor with the largest cathode area demonstrated superior CO_2 utilization compared to the other two reactors. Batch 2 exhibited a trend similar to Batch 1, confirming that increasing the cathode area enhances CO_2 utilization.

3.5. Impact of Cathode Surface Area on Coulombic Efficiency of the MES Process

Figure 6a shows the time-course variations in coulombic efficiency (CE) for three MES reactors with different cathode areas. Although CE fluctuated significantly throughout operation, clear differences among the reactors were evident. The reactor with the

largest cathode area (8 × 16 cm^2) consistently achieved the highest CE values, ranging mostly between 50 and 60%, with several peaks exceeding 60% during the mid-operation phase. This superior performance can be directly associated with the enhanced hydrogen mass transfer capacity provided by the larger electrode surface, which promotes more efficient microbial electron uptake (as discussed in Section 3.2). In contrast, the reactor with the smallest cathode area (8 × 1 cm^2) maintained CE values predominantly in the 30–45% range, rarely surpassing 50%. This lower efficiency aligns with the unfavorable bubble behavior described previously (Section 3.1), where rapid detachment of microbubbles and their reduced residence time in solution limited hydrogen utilization by microbes. The intermediate cathode reactor (8 × 4 cm^2) displayed CE values between the two extremes, mostly within the 40–50% range. Notably, the performance gap between the medium and large cathode reactors widened in later operational stages, suggesting that cathode size becomes increasingly influential as microbial activity stabilizes and acetate accumulation intensifies.

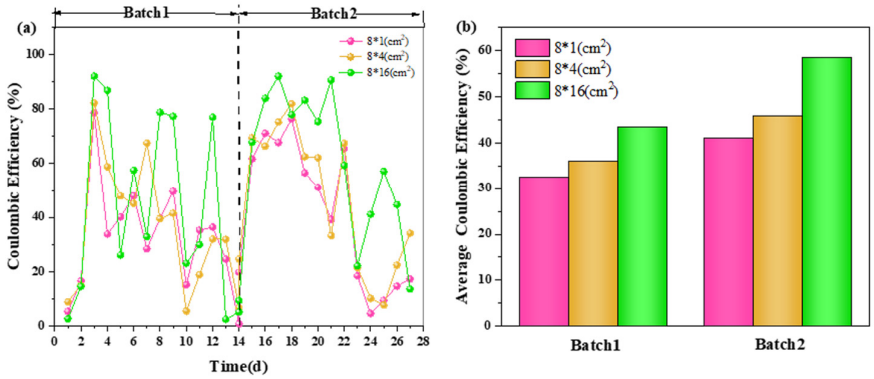


Figure 6. Coulombic efficiency (**a**) and average coulombic efficiency (**b**) for MES reactors with different cathode areas: 8 × 1 cm^2, 8 × 4 cm^2, and 8 × 16 cm^2 (* in figures indicates a multiple sign).

Figure 6b presents the average CE across the three reactors during both batches. In Batch 1, CE values ranged from 33% in the smallest cathode reactor to 43% in the largest cathode reactor. In Batch 2, overall CE increased, with the 8 × 16 cm^2 reactor achieving nearly 59%. These results demonstrate that larger cathode areas improve electron recovery efficiency, consistent with the observed enhancements in H_2 utilization and acetate yield. The improvement is likely due to prolonged bubble residence time and more uniform spatial distribution of hydrogen, which enhances gas–liquid mass transfer and microbial uptake. The higher CE values in Batch 2 further indicate microbial acclimation and improved acetate-producing activity after repeated operation.

Both the dynamic and average CE results consistently demonstrate that increasing the cathode area significantly improves electron recovery efficiency in H_2-mediated MES. The reactor with the largest cathode area (8 × 16 cm^2) achieved the highest average CE (58%) and maintained relatively stable values above 50%, whereas the smallest cathode (8 × 1 cm^2) showed the lowest efficiency (37%) with frequent declines below 30%. The intermediate cathode (8 × 4 cm^2) performed moderately (45%), but its efficiency lagged behind the large cathode, particularly in later stages. These findings confirm that the cathode area is a critical factor regulating hydrogen mass transfer and microbial utilization, though the fluctuations observed also indicate the influence of microbial dynamics and product inhibition on CE stability.

From a practical engineering perspective, although the present study demonstrates that increasing cathode surface area can significantly improve hydrogen mass transfer and acetate production performance in H_2-mediated MES systems, excessively large electrode areas may also introduce practical challenges. Increasing electrode area inevitably raises

material costs and may also influence hydrodynamics within the reactor, potentially affecting mixing efficiency and flow patterns [31]. Therefore, in practical applications, it is necessary to determine an optimal cathode surface area that balances hydrogen mass transfer performance, reactor hydrodynamics, and overall system cost.

In addition, the spatial arrangement of electrodes within the reactor may also play an important role in regulating bubble distribution, gas–liquid mass transfer, and overall reactor performance. Optimizing electrode configuration and placement could further improve hydrogen utilization efficiency without simply increasing electrode area. Consequently, future studies should explore how electrode arrangement, together with cathode surface area, influences gas–liquid mass transfer and microbial utilization in H_2-mediated MES systems, which may provide further insights into reactor design and scale-up.

4. Conclusions

This study systematically investigated the influence of cathode surface area on hydrogen mass transfer and acetate production in a hydrogen-mediated microbial electrosynthesis (MES) system. Under identical operating conditions, increasing the cathode area significantly enhanced hydrogen dissolution and microbial utilization. The reactor equipped with the largest cathode (8×16 cm^2) achieved the highest hydrogen mass transfer coefficient ($k_{La} = 0.592$ h^{-1}), reached hydrogen dissolution equilibrium within approximately 3 min, and produced the highest acetate concentration (32 g L^{-1}), with an average production rate of 2.12 g L^{-1} d^{-1}, hydrogen utilization efficiency of 94%, and coulombic efficiency of 59%. Mechanistic analysis indicates that larger cathode areas promote longer bubble residence times and a more uniform bubble distribution pattern, thereby improving hydrogen availability for microbial metabolism. These results suggest that bubble residence time and spatial distribution, rather than bubble size alone, are key factors governing hydrogen utilization efficiency in H_2-mediated MES systems. From an engineering perspective, optimizing cathode surface area and electrode arrangement are key to balancing gas–liquid mass transfer performance, reactor hydrodynamics, and system cost in future scale-up applications.

Supplementary Materials: The following supporting information can be downloaded at https://www.mdpi.com/article/10.3390/hydrogen7010042/s1. Table S1. Composition of trace metal solution and vitamin solution.

Author Contributions: Conceptualization, K.G. and K.C.; methodology, Y.G., B.W. and H.Z.; validation, Y.G. and J.C.; investigation, Y.G., Y.Y., J.C. and M.Z.; resources, K.G., K.C. and W.C.; data curation, Y.G.; writing—original draft preparation, Y.G.; writing—review and editing, K.G. and S.A.P.; visualization, K.G.; supervision, K.C.; project administration, K.G.; funding acquisition, K.C. All authors have read and agreed to the published version of the manuscript.

Funding: This work was sponsored by the National Natural Science Foundation of China (No. 22578358), The Capability Program Support of Shaanxi (No. 2023-CX-TD-31); Key Research and Development Project of Shaanxi Province (No. 2024CY2-GJHX-73), the open fund from the Xi'an Key Laboratory of C1 Compound Bioconversion Technology, and the Program of Introducing Talents of Discipline to Universities (B23025).

Data Availability Statement: All data and materials are available from the corresponding author upon reasonable request. The data are not publicly available due to ongoing research using a part of the data.

Conflicts of Interest: The authors declare no conflict of interest.

References

1. Chaitanya, N.K.; Rajpurohit, A.; Nair, P.S.; Chatterjee, P. Enhanced carbon capture and medium chain fatty acid production using microbial electrosynthesis: Role of electrode surface area. *Bioresour. Technol.* **2025**, *435*, 132916. [CrossRef] [PubMed]
2. Rabaey, K.; Rozendal, R.A. Microbial electrosynthesis—Revisiting the electrical route for microbial production. *Nat. Rev. Microbiol.* **2010**, *8*, 706–716. [CrossRef] [PubMed]
3. Bian, Y.; Leininger, A.; May, H.D.; Ren, Z.J. H_2 mediated mixed culture microbial electrosynthesis for high titer acetate production from CO_2. *Environ. Sci. Ecotechnol.* **2024**, *19*, 100324. [CrossRef] [PubMed]
4. Ying, Z.; Qiu, Q.; Ye, J.; Chen, H.; Zhao, J.; Shen, Y.; Chu, B.; Gao, H.; Zhang, S. Mechanism, performance enhancement, and economic feasibility of CO_2 microbial electrosynthesis systems: A data-driven analysis of research topics and trends. *Renew. Sustain. Energy Rev.* **2024**, *202*, 114704. [CrossRef]
5. Nevin, K.P.; Woodard, T.L.; Franks, A.E.; Summers, Z.M.; Lovley, D.R. Microbial electrosynthesis: Feeding microbes electricity to convert carbon dioxide and water to multicarbon extracellular organic compounds. *mBio* **2010**, *1*, e00103-10. [CrossRef]
6. Lovley, D.R.; Nevin, K.P. Electrobiocommodities: Powering microbial production of fuels and commodity chemicals from carbon dioxide with electricity. *Curr. Opin. Biotechnol.* **2013**, *24*, 385–390. [CrossRef]
7. Ganesh, I. Electrochemical conversion of carbon dioxide into renewable fuel chemicals—The role of nanomaterials and the commercialization. *Renew. Sustain. Energy Rev.* **2016**, *59*, 1269–1297. [CrossRef]
8. Shen, Q.; Huang, X.; Liu, J.; Guo, C.; Zhao, G. Biomimetic photoelectrocatalytic conversion of greenhouse gas carbon dioxide: Two-electron reduction for efficient formate production. *Appl. Catal. B Environ.* **2017**, *201*, 70–76. [CrossRef]
9. Nitopi, S.; Bertheussen, E.; Scott, S.B.; Liu, X.; Engstfeld, A.K.; Horch, S.; Seger, B.; Stephens, I.E.L.; Chan, K.; Hahn, C.; et al. Progress and Perspectives of Electrochemical CO_2 Reduction on Copper in Aqueous Electrolyte. *Chem. Rev.* **2019**, *119*, 7610–7672. [CrossRef]
10. Hori, Y. Electrochemical CO_2 reduction on metal electrodes. In *Modern Aspects of Electrochemistry*; Springer: New York, NY, USA, 2008; Volume 42, pp. 89–189. [CrossRef]
11. Nevin, K.P.; Hensley, S.A.; Franks, A.E.; Summers, Z.M.; Ou, J.; Woodard, T.L.; Snoeyenbos-West, O.L.; Lovley, D.R. Electrosynthesis of organic compounds from carbon dioxide is catalyzed by a diversity of acetogenic microorganisms. *Appl. Environ. Microbiol.* **2011**, *77*, 2882–2886. [CrossRef]
12. Batlle-Vilanova, P.; Ganigué, R.; Ramió-Pujol, S.; Bañeras, L.; Jiménez, G.; Hidalgo, M.; Balaguer, M.D.; Colprim, J.; Puig, S. Microbial electrosynthesis of butyrate from carbon dioxide: Production and extraction. *Bioelectrochemistry* **2017**, *117*, 57–64. [CrossRef] [PubMed]
13. Vassilev, I.; Hernandez, P.A.; Batlle-Vilanova, P.; Freguia, S.; Krömer, J.O.; Keller, J.; Ledezma, P.; Virdis, B. Microbial Electrosynthesis of Isobutyric, Butyric, Caproic Acids, and Corresponding Alcohols from Carbon Dioxide. *ACS Sustain. Chem. Eng.* **2018**, *6*, 8485–8493. [CrossRef]
14. Bajracharya, S.; Srikanth, S.; Mohanakrishna, G.; Zacharia, R.; Strik, D.P.; Pant, D. Biotransformation of carbon dioxide in bioelectrochemical systems: State of the art and future prospects. *J. Power Sources* **2017**, *356*, 256–273. [CrossRef]
15. James, D.; Shilpa, N.; Freya, B.; Michael, K.; Dennis, S.S. Low-Carbon Fuel and Chemical Production by Anaerobic Gas Fermentation. *Adv. Biochem. Eng. Biotechnol.* **2016**, *156*, 293–321.
16. Drake, H.L.; Gößner, A.S.; Daniel, S.L. Old Acetogens, New Light. *Ann. N. Y. Acad. Sci.* **2008**, *1125*, 100–128. [CrossRef]
17. Bajracharya, S.; Sharma, M.; Mohanakrishna, G.; Benneton, X.D.; Strik, D.P.; Sarma, P.M.; Pant, D. An overview on emerging bioelectrochemical systems (BESs): Technology for sustainable electricity, waste remediation, resource recovery, chemical production and beyond. *Renew. Energy* **2016**, *98*, 153–170. [CrossRef]
18. Pan, Z.; Hu, X.; Cai, W.; Cui, K.; Wang, Y.; Guo, K. An Electrolytic Bubble Column with Gas Recirculation for High-Rate Microbial Electrosynthesis of Acetate from CO_2. *Ind. Eng. Chem. Res.* **2023**, *62*, 16616–16621. [CrossRef]
19. Reguera, G.; McCarthy, K.D.; Mehta, T.; Nicoll, J.S.; Tuominen, M.T.; Lovley, D.R. Extracellular electron transfer via microbial nanowires. *Nature* **2005**, *435*, 1098–1101. [CrossRef]
20. Choi, O.; Sang, B.-I. Extracellular electron transfer from cathode to microbes: Application for biofuel production. *Biotechnol. Biofuels* **2016**, *9*, 11. [CrossRef]
21. Zhu, X.; Jack, J.; Leininger, A.; Yang, M.; Bian, Y.; Lo, J.; Xiong, W.; Tsesmetzis, N.; Ren, Z.J. Syngas mediated microbial electrosynthesis for CO_2 to acetate conversion using *Clostridium ljungdahlii*. *Resour. Conserv. Recycl.* **2022**, *184*, 106395. [CrossRef]
22. Chen, G.; Wang, R.; Sun, M.; Chen, J.; Iyobosa, E.; Zhao, J. Carbon dioxide reduction to high–value chemicals in microbial electrosynthesis system: Biological conversion and regulation strategies. *Chemosphere* **2023**, *344*, 140251. [CrossRef]
23. Shang, G.; Yu, J.; Cai, W.; Cui, K.; Shen, X.; Jin, P.; Guo, K. Comparison of in-situ and ex-situ electrolytic H2 supply for microbial methane production from CO_2. *Bioresour. Technol.* **2023**, *388*, 129728. [CrossRef]
24. Liu, C.; Colón, B.C.; Ziesack, M.; Silver, P.A.; Nocera, D.G. Water splitting–biosynthetic system with CO_2 reduction efficiencies exceeding photosynthesis. *Science* **2016**, *352*, 1210–1213. [CrossRef]

25. Pan, Z.; Liu, Z.; Hu, X.; Cui, K.; Cai, W.; Guo, K. Enhancement of acetate production in hydrogen-mediated microbial electrosynthesis reactors by addition of silica nanoparticles. *Bioresour. Bioprocess.* **2023**, *10*, 3. [CrossRef]
26. Gao, J.-Y.; Cai, W.-F.; Bai, J.-R.; Zhu, Y.-C.; Zhang, Y.-X.; Wang, S.; Guo, K.; Chen, Q.-Y.; Wang, Y.-H. Strengthening H_2 gas–liquid mass transfer using superaerophobic cathodes for enhanced methane production from CO_2 in H_2-mediated microbial electrosynthesis system. *Bioresour. Technol.* **2025**, *417*, 131850. [CrossRef] [PubMed]
27. Jensen, M.B.; Ottosen, L.D.M.; Kofoed, M.V.W. H_2 gas-liquid mass transfer: A key element in biological Power-to-Gas methanation. *Renew. Sustain. Energy Rev.* **2021**, *147*, 111209. [CrossRef]
28. Temesgen, T.; Bui, T.T.; Han, M.; Kim, T.-I.; Park, H. Micro and nanobubble technologies as a new horizon for water-treatment techniques: A review. *Adv. Colloid Interface Sci.* **2017**, *246*, 40–51. [CrossRef] [PubMed]
29. Cai, W.; Cui, K.; Liu, Z.; Jin, X.; Chen, Q.; Guo, K.; Wang, Y. An electrolytic-hydrogen-fed moving bed biofilm reactor for efficient microbial electrosynthesis of methane from CO_2. *Chem. Eng. J.* **2022**, *428*, 132093. [CrossRef]
30. Kantzow, C.; Mayer, A.; Weuster-Botz, D. Continuous gas fermentation by Acetobacterium woodii in a submerged membrane reactor with full cell retention. *J. Biotechnol.* **2015**, *212*, 11–18. [CrossRef]
31. Wu, W.T.; Jong, J.Z. Liquid-phase dispersion in an airlift reactor with a net draft tube. *Bioprocess. Eng.* **1994**, *11*, 43–47. [CrossRef]

Disclaimer/Publisher's Note: The statements, opinions and data contained in all publications are solely those of the individual author(s) and contributor(s) and not of MDPI and/or the editor(s). MDPI and/or the editor(s) disclaim responsibility for any injury to people or property resulting from any ideas, methods, instructions or products referred to in the content.